



Page Proof Instructions and Queries

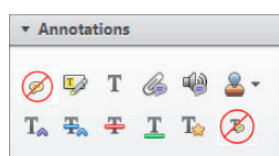
Journal Title: Journal of Mechanical Engineering Science, Proceedings of the Institution of Mechanical Engineers Part C [PIC]

Article Number: 558473

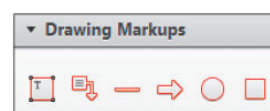
Greetings, and thank you for publishing with SAGE. We have prepared this page proof for your review. Please respond to each of the below queries by digitally marking this PDF using Adobe Reader.

Click "Comment" in the upper right corner of Adobe Reader to access the mark-up tools as follows:

For textual edits, please use the "Annotations" tools. Please refrain from using the two tools crossed out below, as data loss can occur when using these tools.



For formatting requests, questions, or other complicated changes, please insert a comment using "Drawing Markups."




Detailed annotation guidelines can be viewed at: <http://www.sagepub.com/repository/binaries/pdfs/AnnotationGuidelines.pdf>

Adobe Reader can be downloaded (free) at: <http://www.adobe.com/products/reader.html>.

No.	Query
	Please confirm that all author information, including names, affiliations, sequence, and contact details, is correct.
	Please review the entire document for typographical errors, mathematical errors, and any other necessary corrections; check headings, tables, and figures.
	Please confirm that the Funding and Conflict of Interest statements are accurate.
	Please ensure that you have obtained and enclosed all necessary permissions for the reproduction of artistic works, (e.g. illustrations, photographs, charts, maps, other visual material, etc.) not owned by yourself. Please refer to your publishing agreement for further information.
	Please note that this proof represents your final opportunity to review your article prior to publication, so please do send all of your changes now.
AQ: 1	Please provide venue and date of conference for Ref. 4.

Simplified electromagnetic actuation system for three dimensional locomotive and drilling microrobot

Hyunchul Choi, Semi Jeong, Cheong Lee, Gwangjun Go,
Jin Zhen, Seong Young Ko, Jong-oh Park and Sukho Park

Proc IMechE Part C:
J Mechanical Engineering Science
0(0) 1–12
© IMechE 2014
Reprints and permissions:
sagepub.co.uk/journalsPermissions.nav
DOI: 10.1177/0954406214558473
pic.sagepub.com


Abstract

Many researchers have studied and developed various types of medical microrobots using an external electromagnetic field and a permanent magnet. Most microrobots are very small and remotely controlled. Their medical applications include minimally invasive surgery (MIS), capsule endoscopy, drug delivery system (DDS), and cell based therapy. Two-dimensional (2D) or 3D locomotion of microrobots using different electromagnetic actuation (EMA) systems has been studied. In this paper, we propose a simplified EMA system having the same functions as our previous proposed EMA system. Because the simplified EMA system has a smaller coils structure, it consumes less power than the previous EMA system. First, through basic locomotive tests, we demonstrate that the microrobot using the proposed EMA system can move along a desired path in 2D and 3D space. Second, a drilling performance test was carried out on the microrobot. Finally, through quantitative comparison, it was verified that the proposed EMA system consumed 58% less power than the previous EMA system.

Keywords

Microrobot, electromagnetic, 3D locomotion, drilling, Helmholtz coil, saddle coil

Date received: 27 May 2014; accepted: 15 October 2014

Introduction

Various kinds of microrobots actuated through external magnetic field control have been researched for medical applications.^{1–15} Small microrobots in particular were developed for medical applications such as minimally invasive surgery (MIS), capsule endoscopy, drug delivery systems (DDS), and cell based therapy. Generally, external magnetic fields can be generated from permanent magnets or electromagnetic coils.

Fountain et al. proposed a magnetic helical microrobot that was actuated by a magnetic field generated using a permanent magnet. This microrobot was wirelessly controlled through a rotating permanent magnet manipulator.⁴ It was rotated by controlling the external magnetic field and propelled through a rotational spiral tail. Niobe Corporation proposed a magnetic catheter navigation system that used an external controlled permanent magnet.⁵ The active catheter microrobot could change its orientation and was a more effective medical apparatus than the conventional passive catheter. The helical microrobot and

the active catheter microrobot were controlled by manipulating the external permanent magnet using a robotic arm. Therefore, they did not consume power and had no heat problems compared with electromagnetic coil systems.^{4,5} For precise manipulation of microrobots, it is important to regulate the distance between the external permanent magnet and the microrobot. However, the distance regulation in medical applications is very difficult. In addition, because of the large inertia of the external permanent magnet, microrobots respond slowly.

There are several magnetic field generation methods using electromagnetic coils.^{6–15} Martel et al. adopted a magnetic field generated by medical magnetic resonance imaging (MRI) gradient coils to

School of Mechanical Engineering, Chonnam National University, Gwangju, Korea

Corresponding authors:

Jong-oh Park, School of Mechanical Engineering, Chonnam National University, Gwangju 500-757, Korea; Sukho Park, 300 Youngbong-dong, Buk-gu, Gwangju, Korea.
Emails: jop@jnu.ac.kr; spark@jnu.ac.kr

actuate a microrobot. MRI coils manipulated the paramagnetic microrobot and recognized its position at the same time.⁶ They also demonstrated the feasibility of drug delivery using the microrobot in the blood vessel.⁷ However, due to the nature of the MRI system, the degree of freedom (DOF) of the microrobot was constrained and the locomotion of the microrobot was affected by the generated magnetic field during the imaging procedure. Nelson and co-workers proposed a bacterial flagella inspired microrobot and an intraocular microrobot, both of which used an external electromagnetic field.⁸⁻¹⁰ The bacterial flagella inspired microrobot had a spiral shaped body and was propelled by a rotational magnetic field generated by three pairs of orthogonally stationary Helmholtz coils. The intraocular microrobot was actuated by an electromagnetic field generated by the OctoMag magnetic manipulation system.¹⁰ The electromagnetic field could be easily and rapidly controlled through coil current changes. However, the electromagnetic coil system consumed much power and induced heat generation problems.

We previously proposed several types of microrobots that used various electromagnetic actuation (EMA) systems.¹¹⁻¹⁵ The EMA systems were composed from various combinations of Helmholtz coil, Maxwell coil, uniform saddle coil, and gradient saddle coil. Generally, microrobots are aligned in a desired direction by Helmholtz and uniform saddle coils and are propelled along the aligned direction by Maxwell and gradient saddle coils. In addition, the rotational magnetic field generated by the EMA system can rotate the microrobot. Therefore, microrobots of various sizes and shapes can be built according to the locomotive principles and functional purposes. A bullet type microrobot is especially suitable for locomotion in blood vessels, and a spherical type microrobot with a bumpy surface for drilling at occluded parts because of its rotational ability.

Among our proposed EMA systems, the representative EMA system consists of a fixed pair of Helmholtz and Maxwell coils and a rotating pair of uniform and gradient saddle coils.¹² In this paper, we propose a simplified EMA system, which does not have the Maxwell coil that is present in the previous EMA system. That is, the proposed EMA system consists of a fixed pair of Helmholtz coils, and a rotating pair of uniform and gradient saddle coils. Therefore, compared with the previous EMA system, the proposed EMA system can save on power. The uniform magnetic field generated by the Helmholtz and uniform saddle coils can align the microrobot to a desired direction in three dimensional (3D) space and rotate the microrobot for drilling. The gradient saddle coil can generate the propulsion force of the microrobot. In addition, a spherical microrobot with a rough bumpy surface should be used for locomotion and drilling.¹⁴

The main difference of the proposed EMA microrobot system is that the simplified EMA system, without a Maxwell coil, is able to realize similar motions as the previous EMA microrobot systems. Therefore, the simplified EMA system can provide many advantages to solve the power consumption and heating problems when the biomedical microrobots are applied to human bodies. In addition, the simplified EMA system can generate a higher driving force and torque of the microrobot when using the same power supply.

This paper is organized as follows. In “Working principles of proposed EMA system” section, we propose a simplified EMA system and explain the working principles of 3D locomotion and drilling motion of a microrobot using the simplified EMA system. In “Experiments” section, through various experiments, we investigate the 2D and 3D locomotion and drilling performances of the microrobot using the simplified EMA system. Finally, in “Comparative Analysis of Proposed EMA System” section, the power consumption of the proposed EMA system is quantitatively compared with that of the previous EMA system.

Working principles of proposed EMA system

General electromagnetic theory

The generated torque (\mathbf{T} , N·m) and force (\mathbf{F} , N) applied to a magnetic microrobot in a magnetic field are described by the following equations.¹⁶

$$\mathbf{T} = \mu_0 V \mathbf{M} \times \mathbf{H} \quad (1)$$

$$\mathbf{F} = \mu_0 V (\mathbf{M} \cdot \nabla) \mathbf{H} \quad (2)$$

where μ_0 , V , and \mathbf{M} are the magnetic permeability of free space, the volume, and magnetization vector of the magnetic microrobot, respectively.

Generally, Helmholtz and uniform saddle coils are used to generate a uniform magnetic flux and to align the microrobot.¹² The magnetic flux (\mathbf{H}_h , A/m) produced by the x-axis Helmholtz coil is defined as follows:

$$\mathbf{H}_h = [s_h \ 0 \ 0]^T \quad (3)$$

$$s_h = 0.7155 \frac{i_h \times n_h}{r_h} \quad (4)$$

where i_h (A), r_h (m), and n_h are the current, radius of the Helmholtz coil, and turns of coil, respectively. Similarly, the magnetic flux (\mathbf{H}_{us} , A/m) produced by the y-axis uniform saddle coil is defined as follows:

$$\mathbf{H}_{us} = [0 \ d_{us} \ 0]^T \quad (5)$$

$$d_{us} = 0.6004 \frac{i_{us} \times n_{us}}{r_{us}} \quad (6)$$

where $i_{us}(A)$, $r_{us}(m)$, and n_{us} are the current, radius of the uniform saddle coil, and turns of coil, respectively. According to equation (1), the pair of Helmholtz and uniform saddle coils generates a uniform magnetic field in a desired direction and aligns the microrobot along this direction.

Maxwell and gradient saddle coils are used to generate a uniform gradient magnetic field and to propel the microrobot. The magnetic flux ($H_m, A/m$) produced by the x-axis Maxwell coil is defined as follows:

$$\mathbf{H}_m = [g_m x \quad -0.5g_m y \quad -0.5g_m z]^T \quad (7)$$

$$g_m = 0.6413 \frac{i_m \times n_m}{r_m^2} \quad (8)$$

where $i_m(A)$, $r_m(m)$, and n_m are the current, radius of the Maxwell coil, and turns of coil, respectively. The magnetic flux ($H_{gs}, A/m$) produced by the gradient saddle coil is defined as follows:

$$\mathbf{H}_{gs} = [-g_{gs} x \quad 2.4398g_{gs} y \quad -1.4398g_{gs} z]^T \quad (9)$$

$$g_{gs} = 0.3286 \frac{i_{gs} \times n_{gs}}{r_{gs}^2} \quad (10)$$

where $i_{gs}(A)$, $r_{gs}(m)$, and n_{gs} are the current, radius of the gradient saddle coil, and turns of coil, respectively. According to equation (2), the pair of Maxwell and gradient saddle coils generates a uniform gradient magnetic field in a desired direction and propels the microrobot along this direction.

Design and fabrication of simplified EMA system

Recently, we proposed an EMA system for a 3D locomotive microrobot, which consisted of one pair of stationary Helmholtz and Maxwell coils and one pair of rotational uniform and gradient saddle coils.¹² In this paper, we propose a locomotive and drilling microrobot using a simplified EMA system without the Maxwell coil that was present in the previous EMA system.¹² Figure 1 shows an isometric view (a) and a plane view (b) of the proposed EMA system, which consists of a stationary Helmholtz coil along the x-axis and two rotational saddle coils (a uniform saddle coil and a gradient saddle coil) on the x-axis. The Helmholtz coil is a pair of solenoid coils, and is positioned on both sides of the region of interest (ROI). The two saddle coils, with different diameters, are orthogonally positioned on the x-axis, and simultaneously rotated upon the x-axis, as shown in Figure 1.

In Figure 1, α is defined as the angle between the z-axis and the principal axis of the uniform saddle coil (r-axis); the x-r plane is called the working plane of locomotion and drilling of the microrobot. In addition, the gradient and uniform saddle coils are perpendicularly located, and the principal axis of the

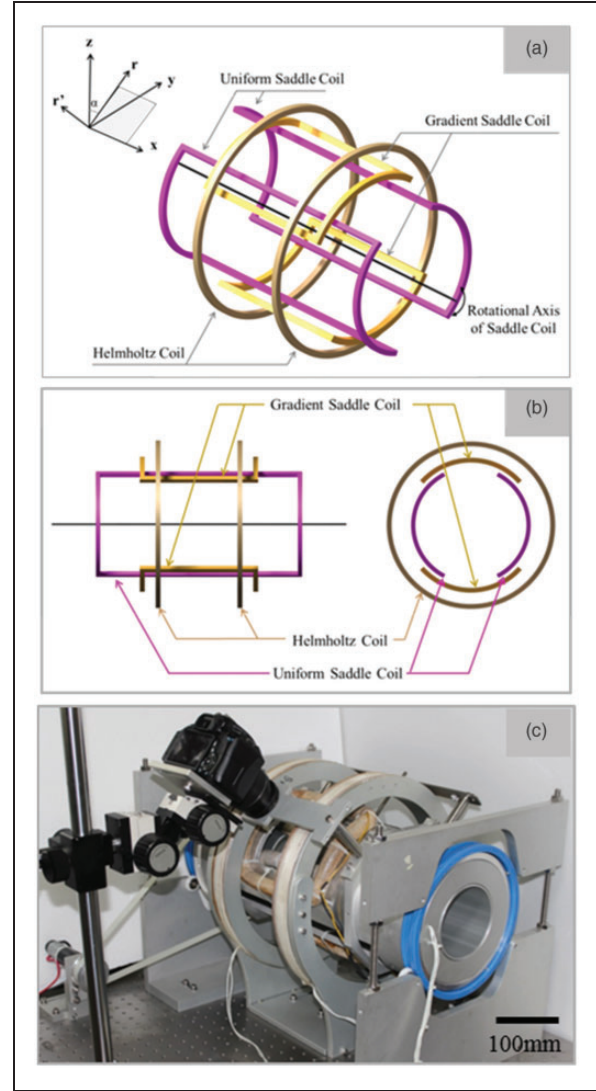


Figure 1. Schematic designs and fabricated proposed EMA system. (a) Isometric view, (b) plane view, and (c) fabricated EMA system.

gradient saddle coil is defined as the r' -axis. Figure 1(c) shows the fabricated EMA system, where uniform saddle and gradient saddle coils are rotated by using a DC motor (Maxon motor, 356846) and a timing belt. The detailed specifications of the fabricated EMA system are shown in Table 1.

2D locomotive mechanism of microrobot

For alignment and locomotion of the microrobot in a 2D plane, α was set to 90° (x-y plane) and the microrobot was aligned to a specific direction and propelled along the desired direction. As shown in Figure 2(a), when the microrobot is aligned in the alignment direction (θ), the x-, y-axis components of magnetization (M) were defined as

$$M_x = -M \cos \theta \quad (11)$$

$$M_y = -M \sin \theta \quad (12)$$

From equations (2) and (9), the propulsion force (F) of the microrobot is determined as

$$F_x = -\mu_0 g_{gs} VM \cos \theta \quad (13)$$

$$F_y = -1.4398 \mu_0 g_{gs} VM \sin \theta \quad (14)$$

From equations (13) and (14), when the locomotion direction of the microrobot is defined as β , the alignment angle (θ) of the microrobot is derived as

$$\frac{F_y}{F_x} = 1.4398 \tan \theta = \tan \beta \quad (15)$$

$$\theta = \tan^{-1} \left(\frac{\tan \beta}{1.4398} \right) \quad (16)$$

Finally, the applied propulsion force of the microrobot and the generated gradient magnetic field in the gradient saddle coil are calculated as

$$F = \frac{-\mu_0 g_{gs} VM \cos \theta}{\sin \beta} \quad (17)$$

$$g_{gs} = -\frac{F \sin \beta}{VM \cos \theta} \quad (18)$$

For 2D locomotion of the microrobot along a desired direction (β), the microrobot is aligned in a specified angle (θ) in equation (16) using the Helmholtz and uniform saddle coils and propelled

Table 1. Specifications of proposed EMA coil system.

Coils	Radius (mm)	Diameter of copper wire (mm)	Coil turns
Helmholtz coil	162.0	1.2	500
Uniform saddle coil	67.0	1.0	419
Gradient saddle coil	140.0	1.0	419

along the desired direction (β) by the gradient magnetic field of the gradient saddle coil in equation (18).

3D locomotive mechanism of microrobot

Through the rotation of the uniform and gradient saddle coils, the 2D locomotive mechanism of the microrobot using the proposed EMA system can be extended to 3D locomotion. In Figure 3, the actuation plane of the EMA system is defined as the x - r plane, where α denotes the angle between z - and r -axis and θ denotes the angle between x -axis and the magnetization direction of the microrobot in the third quadrant.

Based on equations (11) and (12), the x - and r -axes magnetization components of the microrobot can be described as

$$M_x = -M \cos \theta \quad (19)$$

$$M_r = -M \sin \theta \quad (20)$$

Based on equation (9), x - and r -axis components of the magnetic field (\mathbf{H}_{gs}) by the gradient saddle coil are rewritten as

$$\mathbf{H}_{gs} = [-g_{gs}x \quad -1.4398g_{gs}r]^T \quad (21)$$

The propulsion mechanism of the microrobot using the proposed EMA system is shown in Figure 3(c) and (d), where the alignment angle of the microrobot in the x - r plane is defined as θ and the propulsion angle is defined as β . In the 3D locomotion of the microrobot, the effect of the gravitational force should be considered. Because the working plane acts as a floor surface, the normal component ($mg \cos \alpha$) of the gravitational force of the microrobot is cancelled by the reaction force from the working plane, but the tangential component ($mg \sin \alpha$) is not cancelled. Therefore, the tangential component of the gravitational force should be compensated. Similar with

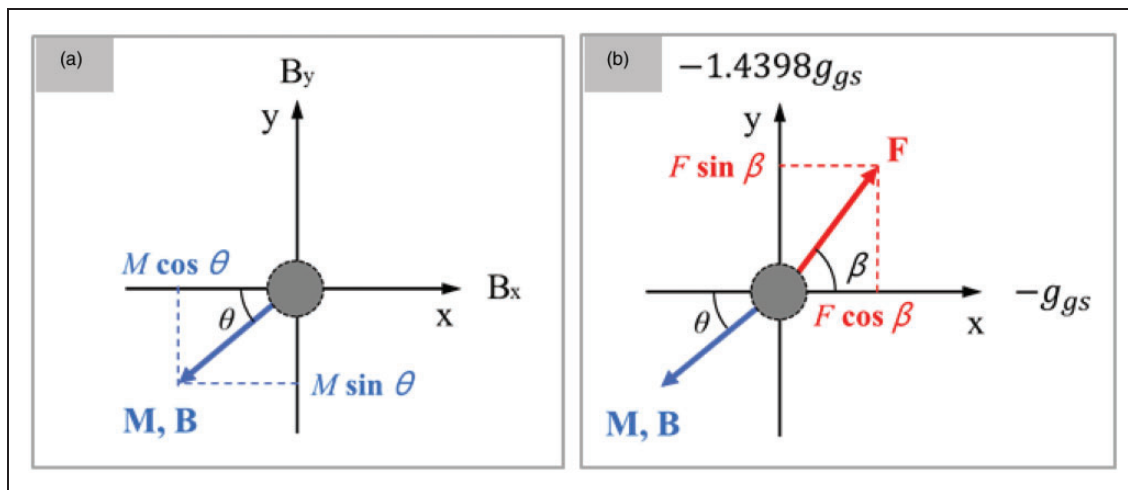


Figure 2. Schematic modeling of 2D locomotion of microrobot. (a) Alignment of microrobot and (b) locomotion of microrobot.

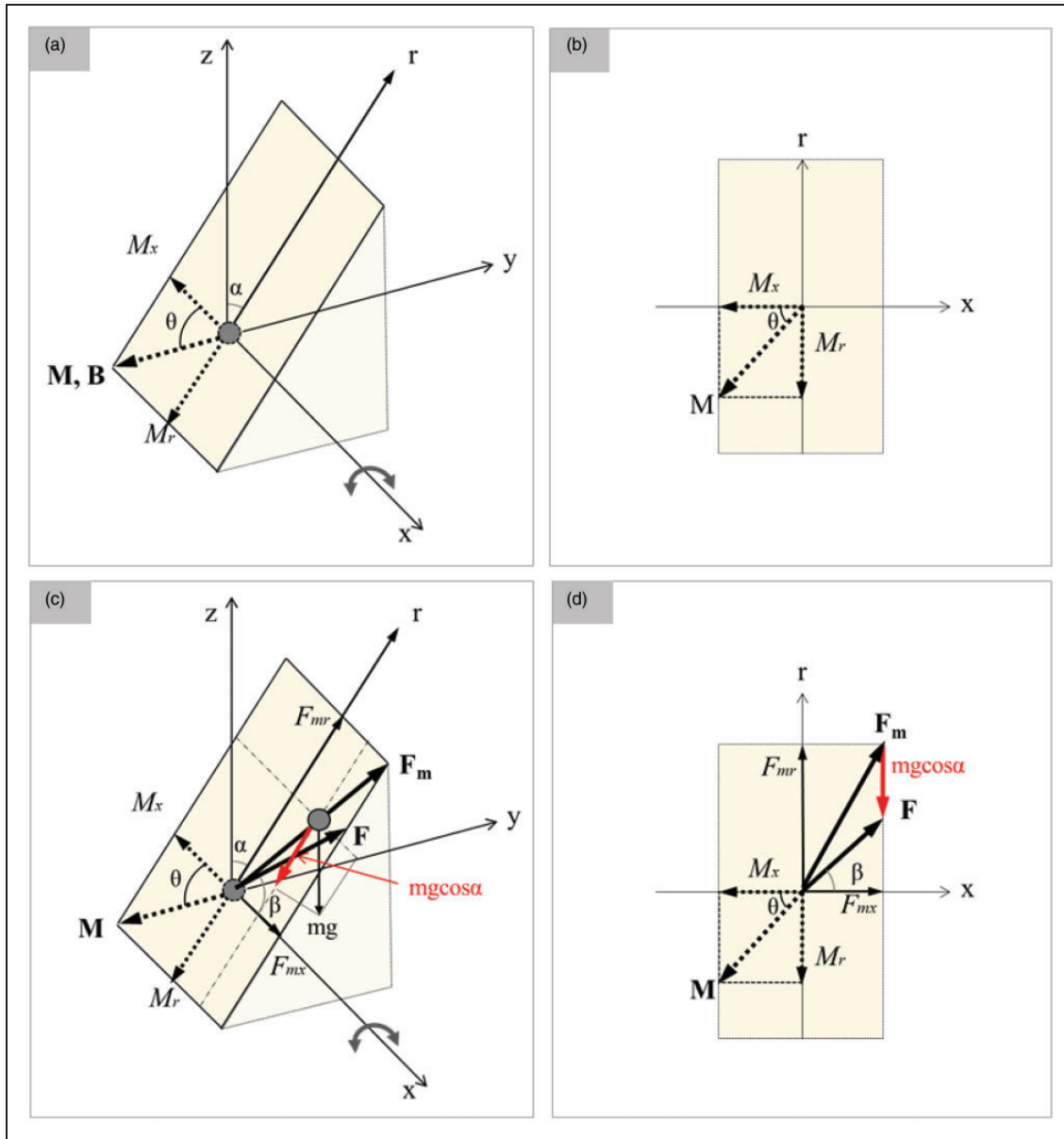


Figure 3. Schematic modeling of 3D alignment and locomotion of the microrobot. (a) Alignment modeling in 3D space, (b) alignment modeling in x-r plane, (c) locomotion modeling in 3D space, and (d) locomotion modeling in x-r plane.

equations (13) and (14), the propulsion forces along x- and r-axes of the microrobot with the consideration of the tangential component of the gravitational force are derived as

$$F_x = -\mu_0 g_{gs} VM \cos \theta = F \cos \beta \quad (22)$$

$$F_r = -1.4398 \mu_0 g_{gs} VM \sin \theta - mg \cos \alpha = F \sin \beta \quad (23)$$

where F_x , F_r , and mg are the x-axis propulsion force, r-axis propulsion force, and the gravitational force of the microrobot, respectively. From equations (22) and (23), the gradient magnetic field (g_{gs}) ingenerated by the gradient saddle coil is calculated as

$$g_{gs} = -\frac{F \cos \beta}{VM \cos \theta} \quad (24)$$

$$g_{gs} = -\frac{mg \cos \alpha + F \sin \beta}{1.4398 VM \sin \theta} \quad (25)$$

Therefore, from equations (24) and (25), the specific alignment direction (θ) of the microrobot can be obtained as

$$\theta = \tan^{-1} \left(\frac{mg \cos \alpha + F \sin \beta}{1.4398 F \cos \beta} \right) \quad (26)$$

Finally, through equations (24) and (26), the gradient magnetic field of the gradient saddle coil can be calculated.

Drilling mechanism of microrobot

As shown in Figure 4, for locomotion and drilling, the microrobot should be spherical shape with rough

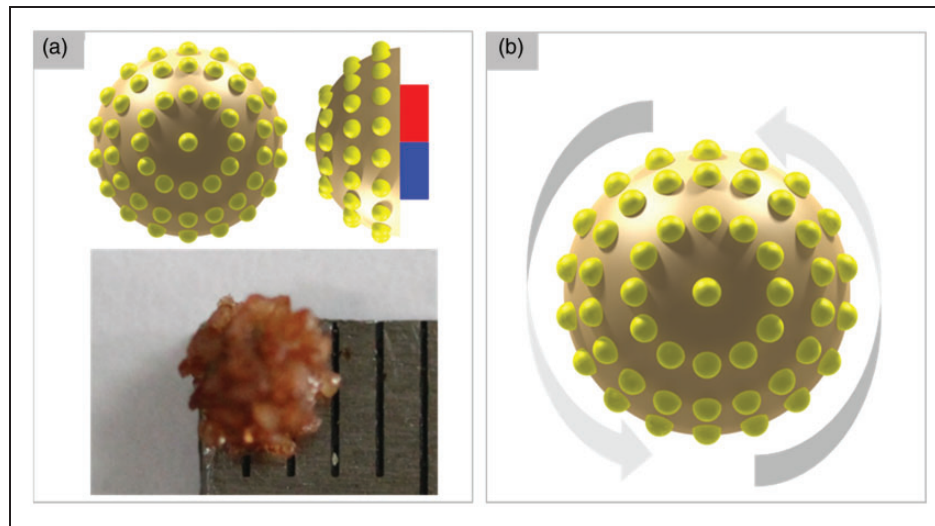


Figure 4. Spherical type microrobot with a rough bumpy surface. (a) Concept design and fabricated microrobot. (b) Rotational motion of microrobot.

bumpy surface and should be able to show separately propulsion motion by a gradient magnetic field and drilling motion by a rotational magnetic field in 3D space.¹⁴ The proposed EMA system has Helmholtz and uniform saddle coils for the alignment and the rotation of the microrobot. Therefore, through these two electromagnetic coils which can generate uniform magnetic fields, the drilling motion of the spherical microrobot with rough bumpy surface can be realized. For the drilling motion of the microrobot, a rotational uniform magnetic field should be generated. Therefore, the following oscillatory magnetic fields should be generated by the Helmholtz coil and the uniform saddle coil.

$$\mathbf{B}_{rot} = [B_0 \cos \omega t \quad B_0 \sin \omega t]^T \quad (27)$$

where B_0 is the magnetic field intensity of the rotational uniform coil and ω becomes the rotational frequency of the microrobot.

As shown in equation (1), when the microrobot is not aligned the uniform magnetic field, the magnetic torque of the microrobot is generated. The magnetic torque exists until the microrobot is aligned with the uniform magnetic field. Therefore, when we use the rotational uniform magnetic field, the microrobot can be rotated. Therefore, the microrobot with rough bumpy surface could realize the drilling function.

Experiments

Experimental setup

As shown in Figure 1(c), we used an experimental setup configuration similar to that of previous papers.^{12–14} The microrobot was located in the ROI, which is the center part of the EMA system. For the observation of the microrobot, a DSLR camera (Canon EOS 600D) was installed on the r' -axis or

on the x-axis. The EMA system controller was composed of a PCIe controller and LabVIEW software (National Instrument), and the coil currents were controlled in joystick mode and manual mode. The currents in the EMA system were applied by three power supplies (MX15–3set, California Instrument). The PCIe controller could communicate with the power supplies using a general-purpose interface bus (GPIB).

Figure 4 shows the spherical type microrobot with a bumpy surface. At the center of the microrobot, a cylindrical permanent magnet of 2 mm in diameter and 2 mm in height was positioned, and SiO_2 particles were attached onto the cylindrical magnet. The final fabricated microrobot has an outer diameter of 3.5 mm and a mass of 0.112 g. Based on the electromagnetic theory, it can be estimated that the proposed EMA microrobot system can generate a maximum torque of 0.135 mN·m, and a maximum driving force of 1.29 mN.

For the 2D and 3D locomotion and drilling tests of the microrobot, we used open loop control methods, where the requisite currents for a desired motion of the microrobot were calculated and applied to the electromagnetic coils. In these experiments, the tracking angle errors were evaluated by the measurement of the angle between the start point and the final point. And, the drilling velocities were calculated through the drilling length and the elapsed time. In addition, the 3D locomotion of the microrobot in blood-vessel phantom was controlled by a master-slave method.

2D locomotion tests of microrobot

To validate the proposed EMA system, 2D locomotion tests were carried out. A spherical neodymium magnet (diameter 2 mm, $M = 955,000 \text{ A/m}$) was used as the microrobot and was positioned in the center of a Teflon dish which was filled with silicone oil of high

viscosity (100 CS). First, basic 2D locomotion tests of the microrobot at the desired directions of 0° , 30° , 45° , 60° , and 90° were performed five times, respectively. The experimental results are shown in Figure 5(a)–(e) and summarized in Figure 5(g). The results showed that the microrobot could precisely move at the desired tracking angles and the 2D tracking angle errors of the microrobot were lower than 1.5° .

From the experimental results in Figure 5(g), it can be seen that the tracking angle errors at the desired directions of 0° and 90° were relatively small

compared with those at the other desired directions. When the desired direction was 0° and 90° , only one coil among the Helmholtz coil and uniform saddle coil was used for the alignment of the microrobot. This demonstrates that alignment using a single coil is less sensitive to the unexpected differences between the two coils, such as resistance variations from Joules heating and manufacturing precision. In addition, alignment errors can also be generated from the force of friction between the microrobot and the bottom surface.

Second, as shown in Figure 5(f), an arbitrary path of 3 mm depth in the Teflon dish was fabricated and used as a desired path for a 2D locomotion test of the microrobot in the joystick control mode. Through Figure 5(f) and Supplementary video, it was verified that the microrobot could move along the predefined path using the proposed EMA system.

3D locomotion test of microrobot

For 3D locomotion tests of the microrobot, we used a rectangular, parallelepiped test bed (width 20 mm, length 20 mm, and height 10 mm) and a spherical permanent magnet microrobot (diameter 2 mm, $M = 955,000$ A/m). For the evaluation of 3D locomotion algorithm, we selected four representative inclined angles ($\alpha = 0^\circ$, 30° , 45° , and 60°), and locomotion tests for four desired direction angles ($\beta = 30^\circ$, 45° , 60° , and 90°) on the surface with the inclined angles were performed, respectively, five times. Figure 6(a)–(d) shows the experimental results on the side with the inclined angle $\alpha = 45^\circ$ and Figure 6(e) shows the summary of the 3D tracking angle errors. The results showed that the microrobot could precisely move at the desired tracking angles and that the 3D tracking angle errors of the microrobot were lower than 1.5° . The tracking angle errors of the microrobot in a 3D space showed even distributions and less variations at the different desired directions and alignment directions. This is due to the lack of frictional force with the bottom surface because the robot was floated, and was able to be precisely aligned and propelled.

Drilling test of microrobot

To evaluate the drilling performance of the microrobot, an acrylic pipe with a 0.3% agar blocked region was used, and the drilling velocity was measured. The oscillatory magnetic fields were generated by the Helmholtz coil and the uniform saddle coil, as described in equation (27), where the magnitude of the magnetic field was 11,040 A/m and the rotational frequencies were changed from 1 Hz to 13 Hz. Figure 7 and the Supplement video show the experimental results of the drilling performance of the microrobot. As the rotational frequency increases to 9 Hz, the drilling velocity linearly increases. However,

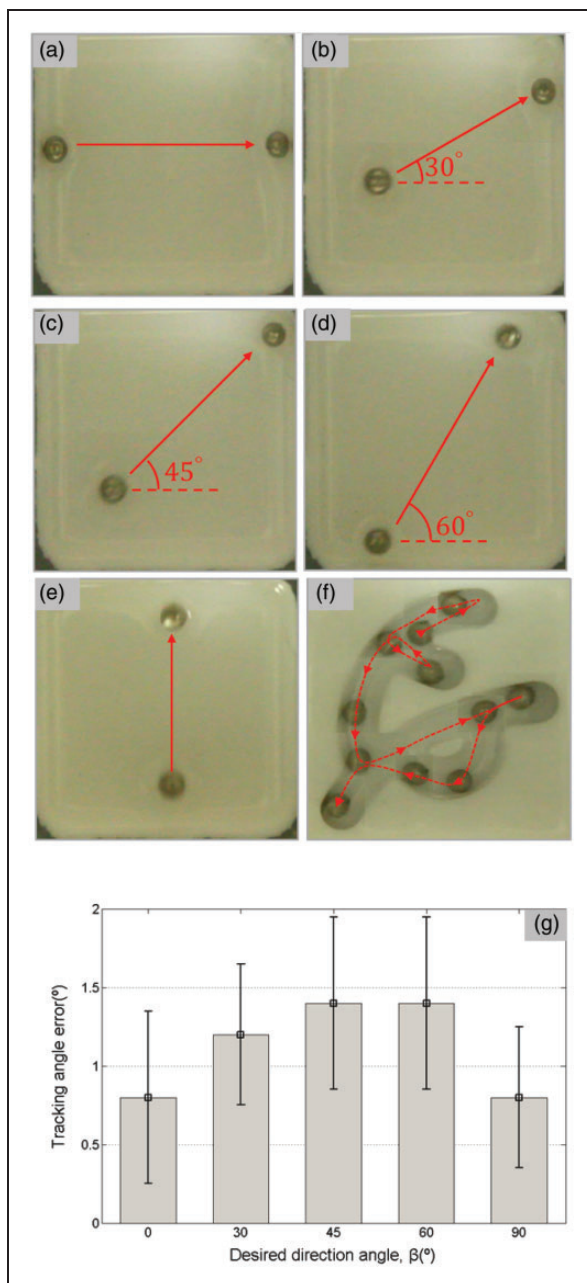


Figure 5. Experimental results. (a)–(e) Basic locomotion of microrobot in 2D plane ($\alpha = 90^\circ$), (f) locomotion of microrobot along 2D desired path ($\alpha = 90^\circ$), and (g) tracking angle errors of 2D locomotion test. Values are expressed as mean \pm SE.

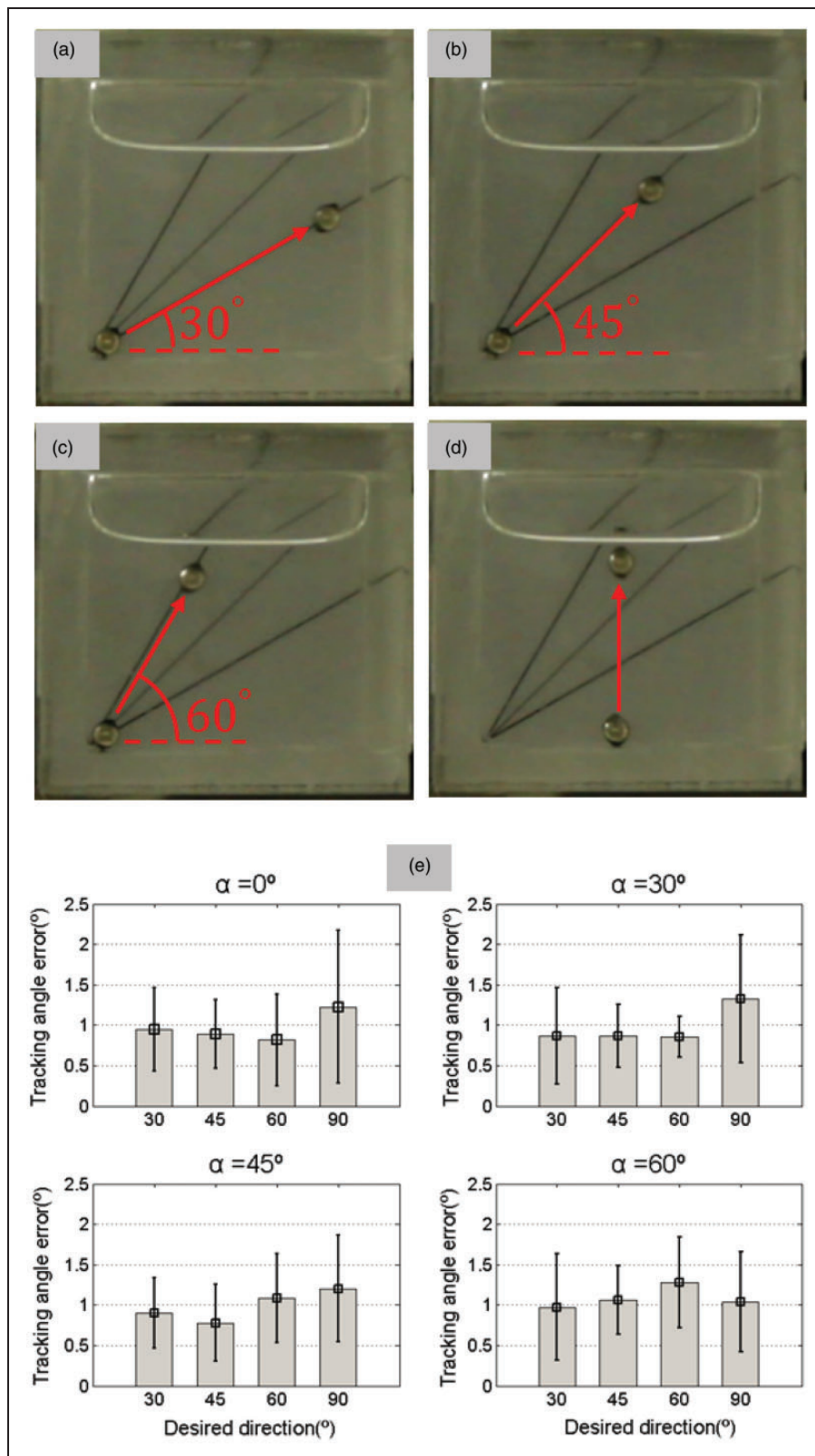


Figure 6. Experimental results. (a)–(d) Locomotion of microrobot in 3D space ($\alpha = 45^\circ$) and (e) tracking angle errors of 3D locomotion test. Values are expressed as mean \pm SE.

at higher rotational frequencies over 9 Hz, the drilling velocity decreased. The EMA coils can be regarded as R-L circuits. Therefore, as the driving frequencies increase in the low frequency region, the drilling

velocity of the microrobot increases. However, a reverse of this tendency was observed in the high driving frequency region (>10 Hz). Similar phenomena were found in previous studies.^{17,18} Furthermore,

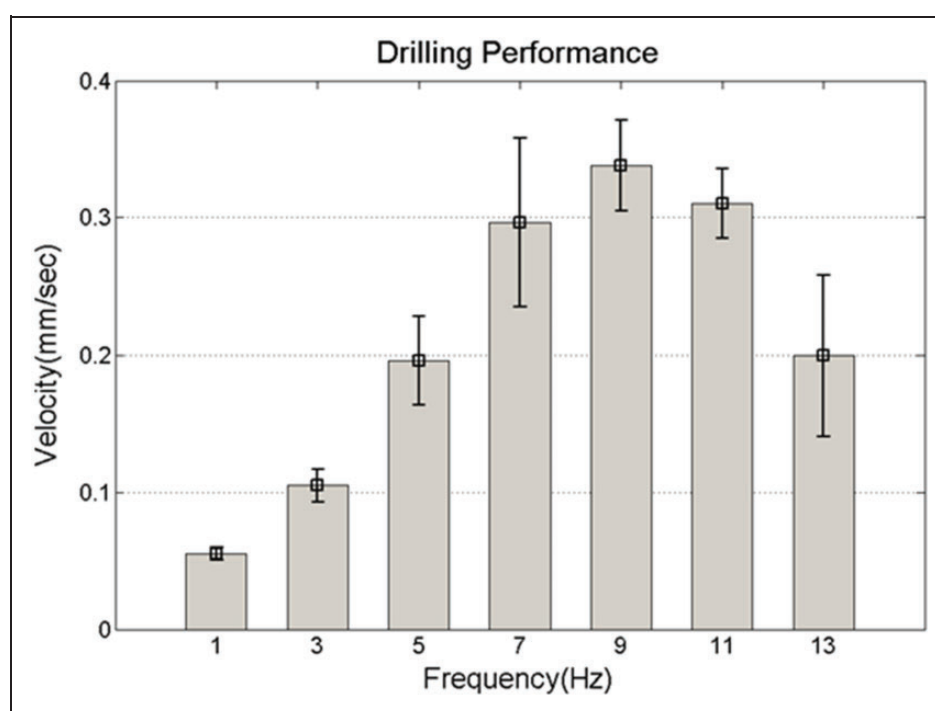


Figure 7. Drilling velocities of microrobot. Values are expressed as mean \pm SE.

drilling efficiency decreased when the rotational frequency exceeded a specific frequency (step-out frequency).^{17,18} Therefore, the step-out frequency of the proposed EMA system was about 9 Hz.

Through these experiments, it was verified that the proposed microrobot shows a drilling motion due to the rotation of its bumpy surface. The drilling motion could be an important mechanism for providing therapeutic functions in blood vessel microrobots. In addition, we expect that the drilling motion of the microrobot could have uses for the treatment of various diseases, such as hydrocephalus and tumors.

3D locomotion and drilling test of microrobot in blood-vessel phantom

The 3D locomotion and drilling of the microrobot were confirmed by using a phantom of human blood vessels. From computed tomography (CT) images of human blood vessels, the rendering data of the blood vessels were extracted. Based on the rendering data, a blood-vessel phantom was fabricated by a rapid prototype (RP) process.¹⁴ The phantom was a cubic shape of 40 mm, and blood vessels of 4 mm in diameter 4 mm. It also had vascular routes of about 45° ascending slope and about 45° descending slope. The vessels of the phantom were filled with silicone oil (100 CS) and a branch vessel was filled with 0.3% agar as an occlusion model. For the locomotion and drilling tests, a spherical microrobot with a bumpy surface was used.¹² The 3D locomotion and drilling results of the microrobot in the blood-vessel phantom are shown in Figure 8 and Supplement video.

The experimental results showed that the microrobot could move along 3D path and drill the occlusion model in the blood-vessel phantom.

Comparative analysis of proposed EMA system

As shown in Figure 9, the proposed EMA system (Figure 9(b)) has a structure without the Maxwell coil that is present in the previous EMA system (Figure 9(a)).¹² In this section, we compare these two EMA systems with respect to power consumption. These two EMA systems have identically same Helmholtz coils and uniform saddle coils and the same actuation mechanism for the alignment of the microrobot.¹² Therefore, we did not consider the power consumptions of Helmholtz coils and uniform saddle coils, and the uniform coils structure but considered their different gradient coils namely, the gradient saddle coils and Maxwell coils. For a reasonable comparison, the following assumptions⁹ were introduced.

- For the geometrical arrangement of the gradient saddle coil and Maxwell coil in the previous EMA system, the radius of Maxwell coil should be slightly larger than that of the gradient saddle coil. In addition, the Maxwell coil can have a same radius as the Helmholtz coil, which is arranged in a same axis. Therefore, the radii of the Helmholtz coil and Maxwell coil were determined to be 1.157 times larger than that of the gradient saddle coil.

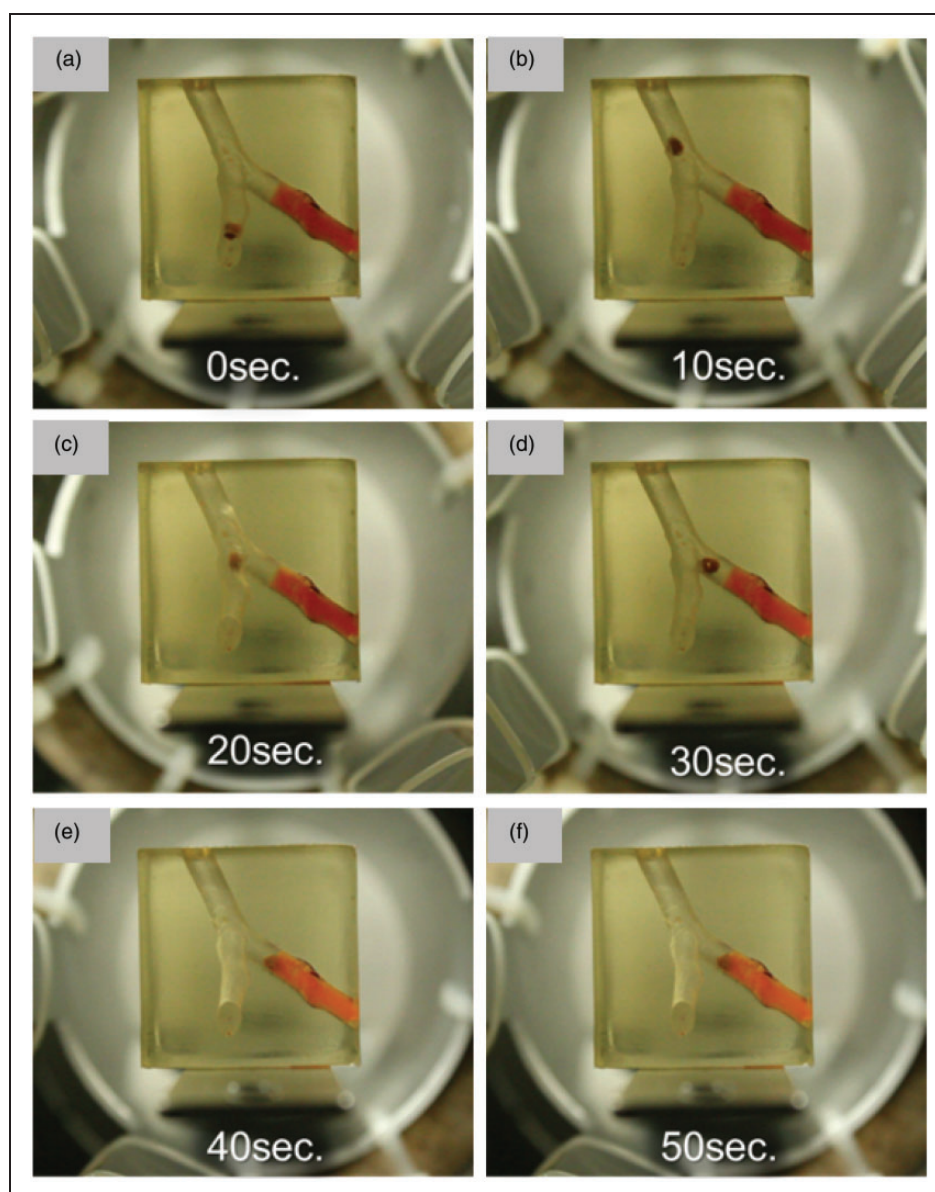


Figure 8. Locomotion and drilling test of microrobot in blood-vessel phantom.

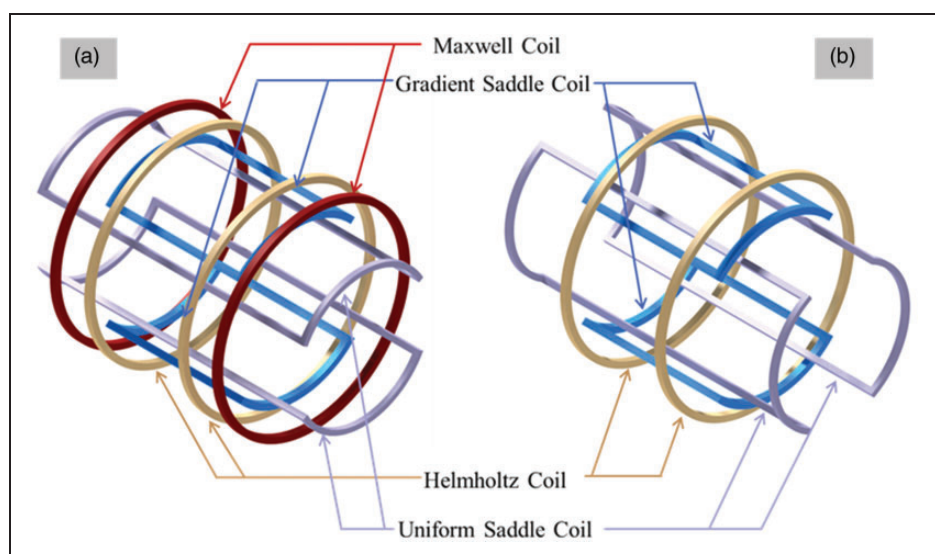


Figure 9. Schematic diagram of two EMA systems. (a) Previous EMA system and (b) proposed EMA system.

Table 2. Comparison of power consumption between two EMA systems.

	Previous system		Proposed system
	MC	GSC-1	GSC-2
Radius ratio	1.157	1	1
Winding number ratio	1.568	1	1
Resistance ratio	22.798	13.371	13.371
Current ratio	1	1	1.059
Gradient magnetic field	0.751	0.329	0.348
Average gradient magnetic field	0.424		0.424
Power consumption	36.169		14.995

- In the previous EMA system, we determined the winding number ratio of Maxwell coil, at which the microrobot was propelled in the aligned direction with the current in Maxwell coils equal to that in the gradient saddle coils. In addition, the gradient saddle coil in the proposed EMA system had the same winding number of the gradient saddle coil in the previous EMA.
- For the actuation of the microrobot in the desired direction in 2D plane, the two EMA systems have the same average gradient magnetic field.

Based on these assumptions, the comparison results are shown in Table 2. The comparative analysis verified that the proposed EMA system can consume 58% less power than the previous EMA system. Therefore, compared with the previous EMA system, the proposed EMA microrobot can be actuated by substantially less power. When using the same power input, our microrobot can show enhanced performance, including larger driving force and torque, and precise tracking accuracy.

Conclusions

In this study, we proposed a simplified EMA system for 3D locomotion and drilling of the microrobot. Although the proposed EMA system has the same functions as the previous EMA system,¹⁰ it has a structure without the Maxwell coil that is present in the previous EMA system. First, we proposed the 2D and 3D locomotion and drilling mechanisms of the microrobot using the proposed EMA system. Second, through various experiments using test beds and a blood-vessel phantom, we verified the tracking and drilling performance of the microrobot. Finally, we found that the proposed EMA system can consume much less power than the previous EMA system.

The proposed EMA microrobot, which shows precise locomotion in 2D and 3D space, can be used for

specific drug delivery. In addition, because it can be applied to the manipulation of cells and micro-particles, it can also be used for cell study using micro-fluidic chips. In the future, through enhancements of the therapeutic functions, the position recognition and the controllability of the microrobot, we expect that the microrobot will be widely utilized for various biomedical applications.

Conflict of interest

None declared.

Funding

This work was supported by a Grant-in-Aid for Strategy Technology Development Programs (No. 10030037) from the Korea Ministry of Knowledge Economy.

References

1. Nelson BJ, Kaliakatsos I and Abbott JJ. Microrobots for minimally invasive medicine. *Annu Rev Biomed Eng* 2010; 12: 55–85.
2. Abbott JJ, Nagy Z, Beyeler F, et al. Robotics in the small-part I: microrobotics. *IEEE Robot Autom Mag* 2007; 14: 92–103.
3. Ishiyama K, Sendoh M and Arai K. Magnetic micro-machines for medical applications. *J Magn Magn Mater* 2002; 242–245: 41–46.
4. Fountain TWR, Kailat PV and Abbott JJ. Wireless control of magnetic helical microrobots using a rotating-permanent-magnet manipulator. In: *IEEE international conference on robotics and automation (ICRA)*, 2010.
5. Ramcharitar S, Patterson MS, Geuns RJv, et al. Technology insight: magnetic navigation in coronary interventions. *Nat Clin Pract Cardiovasc Med* 2008; 5: 148–156.
6. Martel S, Felfoul O, Mathieu JB, et al. MRI-based medical nanorobotic platform for the control of magnetic nanoparticles and flagellated bacteria for target interventions in human capillaries. *Int J Robot Res* 2009; 28: 1169–1182.
7. Pouponneau P, Leroux JC and Martel S. Magnetic nanoparticles encapsulated into biodegradable micro-particles steered with an upgraded magnetic resonance imaging system for tumor chemoembolization. *Biomaterials* 2009; 30: 6327–6332.
8. Kummer MP, Abbott JJ, Kratochvil BE, et al. OctoMag: an electromagnetic system for 5-DOF wireless micromanipulation. *IEEE Trans Robot* 2010; 26: 1006–1017.
9. Zhang L, Abbott JJ, Dong L, et al. Artificial bacterial flagella: fabrication and magnetic control. *Appl Phys Lett* 2009; 94: 064107–064107.
10. Zhang L, Peyer KE and Nelson BJ. Artificial bacterial flagella for micromanipulation. *Lab Chip* 2010; 10: 2203–2215.
11. Choi H, Choi J, Jeong S, et al. Two-dimensional locomotion of a microrobot with a novel stationary electromagnetic actuation system. *Smart Mater Struct* 2009; 18: 1–6.
12. Choi H, Cha K, Choi J, et al. EMA system with gradient and uniform saddle coils for 3D

- locomotion of microrobot. *Sens Actuat A Phys* 2010; 63: 410–417.
13. Jeong S, Choi H, Cha K, et al. Enhanced locomotive and drilling microrobot using precessional and gradient magnetic field. *Sens Actuat A Phys* 2011; 171: 429–435.
14. Choi H, Cha K, Jeong S, et al. 3-D locomotive and drilling microrobot using novel stationary EMA system. *IEEE/ASME Trans Mechatron* 2013; 18: 1221–1225.
15. Go G, Choi H, Jeong S, et al. Position-based magnetic field control for an electromagnetic actuated microrobot system. *Sens Actuat A Phys* 2014; 205: 215–223.
16. Hayt WH and Buck JA. *Engineering electromagnetic*. 7th ed. New York: McGraw-Hill, 2006.
17. Yamazaki A, Sendoh M, Ishiyama K, et al. Three-dimensional analysis of swimming properties of a spiral-type magnetic micro-machine. *Sens Actuat A Phys* 2003; 105: 103–108.
18. Zhang L, Abbott JJ, Dong L, et al. Characterizing the swimming properties of artificial bacterial flagella. *Nano Letters* 2009; 9: 3663–3667.